

RESEARCH PAPER



# H1N1 influenza virus dose dependent induction of dysregulated innate immune responses and STAT1/3 activation are associated with pulmonary immunopathological damage

Duoduo Yao<sup>a</sup>, Linlin Bao<sup>b</sup>, Fengdi Li<sup>b</sup>, Bo Liu<sup>c</sup>, Xu Wu<sup>d</sup>, Ziqi Hu<sup>a</sup>, Jiangnan Xu<sup>a</sup>, Wei Wang<sup>a</sup>, and Xulong Zhang<sup>a,e</sup>

<sup>a</sup>Department of Immunology, School of Basic Medical Sciences, Capital Medical University, Beijing, China; <sup>b</sup>NHC Key Laboratory of Human Disease Comparative Medicine (The Institute of Laboratory Animal Sciences, CAMS&PUMC), Beijing Key Laboratory for Animal Models of Emerging and Reemerging Infection, Beijing, China; <sup>c</sup>Department of Pulmonary and Critical Care Medicine, Department of Clinical Microbiology, Zibo City Key Laboratory of Respiratory Infection and Clinical Microbiology, Zibo City Engineering Technology Research Center of Etiology Molecular Diagnosis, Zibo Municipal Hospital, Zibo, China; <sup>d</sup>Department of Respiratory Medicine, Hunan Provincial People's Hospital (The First Affiliated Hospital of Hunan Normal University), Changsha, China; <sup>e</sup>Beijing Key Laboratory of Cancer Invasion and Metastasis Research, School of Basic Medical Sciences, Capital Medical University, Beijing, China

## ABSTRACT

Influenza A virus (IAV) infection poses a substantial challenge and causes high morbidity and mortality. Exacerbated pulmonary inflammatory responses are the major causes of extensive diffuse alveolar immunopathological damage. However, the relationship between the extent of cytokine storm, neutrophils/macrophages infiltration, and different IAV infection dose and time still needs to be further elucidated, and it is still unclear whether the signal transduction and transcriptional activator 1/3 (STAT1/3) signalling pathway plays a beneficial or detrimental role. Here, we established a mouse model of high- and low-dose pH1N1 infection. We found that pH1N1 infection induced robust and early pathological damage and cytokine storm in an infection dose- and time-dependent manner. High-dose pH1N1 infection induced massive and sustained recruitment of neutrophils as well as a higher ratio of M1:M2, which may contribute to severe lung immunopathological damage. pH1N1 infection activated dose- and time-dependent STAT1 and STAT3. Inhibition of STAT1 and/or STAT3 aggravated low-dose pH1N1 infection, induced lung damage, and decreased survival rate. Appropriate activation of STAT1/3 provided survival benefits and pathological improvement during low-dose pH1N1 infection. These results demonstrate that high-dose pH1N1 infection induces robust and sustained neutrophil infiltration, imbalanced macrophage polarization, excessive and earlier cytokine storm, and STAT1/3 activation, which are associated with pulmonary dysregulated proinflammatory responses and progress of acute lung injury. The severe innate immune responses may be the threshold at which protective functions give way to immunopathology, and assessing the magnitude of host innate immune responses is necessary in adjunctive immunomodulatory therapy for alleviating influenza-induced pneumonia.

## ARTICLE HISTORY

Received 7 May 2022  
Revised 29 July 2022  
Accepted 31 August 2022

## KEYWORDS

STAT1; STAT3; acute lung injury; H1N1; innate immune; viral pneumonia

## Introduction

Influenza A virus (IAV) is a highly infectious respiratory pathogen. Severe pandemic influenza A (H1N1) 2009 virus (pH1N1) and H3N2 epidemics are responsible for more than 5 millions infection worldwide and approximately 500,000 deaths annually [1]. Occasional pandemics of H1N1 infection causes high morbidity and mortality worldwide, presenting a great threat to international public health security [2]. Our clinical data and mouse model experiments revealed that severe pH1N1 infection presents with rapidly progressive pneumonia characterized by extensive and diffuse alveolar damage, acute respira-

tory distress syndrome, and even multiple organ failure, which causes significant mortality [3,4]. IAV can directly infect and destroy lung epithelial cells and alveolar macrophages to induce immune responses and acute lung injury. A rational immune response may help eliminate the influenza virus and maintain immune homeostasis. However, we and others have found that excessive immune response-induced immunopathological damage plays a critical role in the pathogenesis of severe pneumonia [4–6]. Comparison of IAV-induced innate immune responses at indicated days post infection (dpi) with different infectious doses is helpful to elucidate

**CONTACT** Wei Wang  [wy\\_robin@ccmu.edu.cn](mailto:wy_robin@ccmu.edu.cn); Xulong Zhang  [zhxlwl@ccmu.edu.cn](mailto:zhxlwl@ccmu.edu.cn)

© 2022 The Author(s). Published by Informa UK Limited, trading as Taylor & Francis Group.  
This is an Open Access article distributed under the terms of the Creative Commons Attribution-NonCommercial License (<http://creativecommons.org/licenses/by-nc/4.0/>), which permits unrestricted non-commercial use, distribution, and reproduction in any medium, provided the original work is properly cited.

immunopathology and may provide potential targets and strategies for the treatment of severe IAV infection.

Evidence has shown that dysregulated innate immune responses are closely related to high mortality. IAV infection-induced cytokines play different roles at different stages of infection. At the early stage, appropriate levels of cytokines protect the host against viral infections. But excessive production of pro-inflammatory cytokines, also termed “cytokine storm,” have been regarded as the crucial reason for the lethal clinical symptoms by causing a cascade of amplified inflammatory effects [5,7]. In addition to specific elevated cytokine levels, host or pathogen factors may also be important in defining “cytokine storms” [8]. The level of pro-inflammatory cytokines is significantly increased during influenza virus infection, including interleukin-6 (IL-6), interferon (IFN), tumour necrosis factor (TNF), and chemokines [9]. The level of IFN- $\alpha/\beta$  or IFN- $\gamma$  production is the pivotal innate immune defence response against viral infections, and IFN- $\gamma$  plays an important role in the early stage of antiviral response [10,11]. IFN not only blocks virus replication by producing antiviral mediators, but it also aggravates the immunopathological damage when it is dysregulated [12]. The beneficial or detrimental effects may be depended on the time and dose of infection.

Following viral infection, monocytes/macrophages and neutrophils are the main innate immune cells recruited into alveoli at the early stage of infection [13]. Not only can monocytes/macrophages phagocytose infected target cells, but they also can secrete different cytokines by differentiating into different subsets. Classically activated macrophage (M1) and alternatively activated macrophage (M2) are the most common macrophage subtypes [14]. M1 cells polarized at the early stage of infection can secrete high amounts of pro-inflammatory cytokines, which may play protective or immunopathological effects depending on their concentrations and maintenance time [15]. M2 cells play roles in inhibiting inflammation and repairing tissue. The ratio of M1 to M2 changes continuously until the pathogen is completely eliminated and tissue repair reaches homeostasis [16–18]. Dysregulated M1/M2, such as the excessive activation of M1 cells, can lead to severe inflammatory factor storms and tissue damage [19]. Investigating the changes and ratios of M1 and M2 in the lungs at different infection times and doses will help to regulate immunopathological damage.

As the central actor of IFN in inflammation response, signal transducer and activator of transcription (STAT) plays a key actor in natural immunity by

directing the transcriptional response to IFNs and other cytokines, thereby provoking antiviral responses and inflammatory responses [20,21]. STAT1 and STAT3 can be activated by IFNs and IL family cytokines, including IFN- $\alpha/\beta/\gamma$ , IL-6, G-CSF, and IL-21 [22]. In addition, STAT1 also participated in the polarization of macrophages to M1 [23,24]. STAT3 was involved in the M2 polarization [25]. Furthermore, STAT1 deficiency could exacerbate the pathological damage of IAV [26]. But our and other previous results demonstrated that neutralizing IFN $\gamma$  improved survival and reduced lung injury in mice with the high-dose of  $10^6$ /ml 50% tissue culture infective doses (TCID<sub>50</sub>) pH1N1 infection [27,28]. Investigating the expression and activity of STAT1 and STAT3 in the lungs at different infection doses and times will help further identify their beneficial or harmful functions and determine potential therapeutic drugs and the appropriate time of administration for influenza treatment.

Here, we established a mouse model of pH1N1 infection with different infectious doses. We found that high-dose influenza virus infection induces more severe pathological damage, accompanied by higher numbers and more sustained neutrophil infiltration, more imbalanced macrophage subsets, a stronger and earlier cytokine storm, and STAT1/3 activation. The inhibition of STAT1 or/and STAT3 with Fludarabine, C188–9, and Stattic decreased survival rate and increased lung damage at low-dose pH1N1 infection. Thus, our results show that high-dose pH1N1 infection induced by stronger and earlier innate immune responses may mediate pulmonary immunopathological damage, and STAT1 and STAT3 activation may be beneficial for low-dose pH1N1 infection.

## Materials and methods

### *Mice, influenza virus*

Female BALB/c mice (specific pathogen-free, 6–8 weeks) and pH1N1 were donated from the Institute of Laboratory Animal Science (Peking Union Medical College, China).

### *Influenza virus infection*

Mice were anesthetized and inoculated intranasally with  $10^2$  and  $10^6$  TCID<sub>50</sub> of pH1N1 virus in a volume of 50  $\mu$ l. Control group was treated with an equal volume of phosphate-buffered saline. After infection, the weight and the survival of mice were monitored for 14 dpi or until death.

### **Virus titrations**

The homogenized lung tissues were collected, then virus titrations were performed by end-point titration in MadinDarby canine kidney cells and calculated using the Reed-Muench method [4].

### **Inhibitors treatment**

Fludarabine (Selleck, TX, USA), C188-9 (Selleck, TX, USA), or Stattic (Selleck, TX, USA) was administered by intraperitoneal injection alone or combined with Oseltamivir (Roche, Basel, Switzerland) administered by gavage once per day from 2 dpi for 7 days. The dose for Oseltamivir was 30 mg/kg. For the mice treated with Fludarabine, C188-9, or Stattic alone or combined with Oseltamivir, a double dose of 100 µg/kg, 40 µg/kg, and 20 µg/kg was used to achieve the steady-state blood concentrations on the first day. A maintenance dose of 50 µg/kg, 20 µg/kg, and 10 µg/kg, respectively, was administered during the following 6 days. Control group was treated with an equal volume of PBS.

### **Haematoxylin and eosin staining (H&E) and histopathological assessment**

The whole lung was fixed with 4% paraformaldehyde and embedded in paraffin. Panoramic SCAN 150 (3DHISTECH, Budapest, Hungary) was used to observe the sections. Ten fields of view were selected from the scanned whole slides randomly and then analysed by CaseViewer software (3DHISTECH, Budapest, Hungary). Lung injury score was assessed using a semiquantitative scoring system [29]. The degree of oedema, interstitial and alveolar haemorrhage, atelectasis, and pulmonary septum thickening were scored according to the following scale: 0 = no injury, 1 = injury in 25% of the field, 2 = injury in 50% of the field, 3 = injury in 75% of the field, and 4 = injury throughout the field. Infiltration scores were assessed according to the infiltration degree of inflammatory cells surrounding three large vessels and the main bronchus: 0 = no inflammatory cells, 1 = a few inflammatory cells, 2 = more uneven distribution of inflammatory cells, 3 = a large number of inflammatory cells distributed relatively evenly and rarely gathered into a clump, 4 = a large number of inflammatory cells congregated [30]. Results were analysed in blinded by an experienced pathologist.

### **Immunohistochemical staining**

Deparaffinized and hydrated of paraffin-embedded lung sections. The expression of haemagglutinin (HA) and the activation of STAT pathway were assessed using anti-HA (1:2000; Sino Biological), anti-pSTAT1 (Tyr701) antibody (1:200, Cell Signalling Technology, MA, USA) and anti-pSTAT3 (Tyr705) antibody (1:200, Cell Signalling Technology). Macrophage infiltration was explored using anti-F4/80 antibody (1:200, Cell Signalling Technology). Neutrophil recruitment was assessed using anti-Ly6G antibody (1:200, Cell Signalling Technology). The antibody was detected by streptavidin-biotin (Beijing Zhongshan Biotechnology Co., Ltd., Beijing, China). Five slides were randomly selected from the whole slides, and then evaluated using Image J pro.

### **Obtaining of bronchoalveolar lavage fluid (BALF)**

The lung was lavaged with 2 × 1 ml of PBS. The BALF was centrifuged 1500 rpm at 4°C for 10 min, and the supernatant was obtained and stored at -80°C.

### **Cytokine and chemokine analysis**

The IL-6, IFN-α/β/γ, IL-1β, IL-10, IL-12 (p70), IL-17A, IL-21, IL-23, IL-28, CXCL1, CCL2, CCL3, TNF-α, G-CSF, and GM-CSF levels in 50 µl of BALF or serum were assessed by Bio-Plex Mouse Cytokine Panel Assay Kit (Bio-Rad Laboratories, CA, USA).

### **Flow cytometry analysis**

The whole lung was cut into pieces with ophthalmic scissors. The tissue was incubated with 0.1% type I collagenase (Sigma, MO, USA) at 37°C for 60 min. Then, the cells were homogenized through a 70 µm cell strainer (BD Biosciences). Isolated cells from lung tissue of mice were first incubated with FVS510 (BD Biosciences, CA, USA) for 15 min. After washing two times with 2% FBS, cells were incubated with monoclonal antibody against CD16/CD32 (BD Pharmingen, CA, USA) for 10 min to block Fc receptors. Next, cells were stained with BB515-anti-CD45 (BD Biosciences), BV421-anti-F4/80 (BD Biosciences), BV711-anti-Ly6G (BD Biosciences), APC-anti-CD11b (BD Biosciences), and PerCP-Cy5.5-anti-MHC-II (BD Biosciences) at 4°C for 20 min. The cells were fixed and permeabilized with 200 µl Perm/Wash Buffer (BD Biosciences). Intracellular staining of BV605-anti-CD206 antibody (BD Biosciences) was incubated at 4°C for 40 min. Specific cell types were identified as follows: neutrophil

(CD45<sup>+</sup>CD11b<sup>+</sup>Ly6G<sup>+</sup>), macrophage (CD45<sup>+</sup>F4/80<sup>+</sup>), M1 macrophage (CD45<sup>+</sup>F4/80<sup>+</sup>MHC-II<sup>+</sup>), M2 macrophage (CD45<sup>+</sup>F4/80<sup>+</sup>CD206<sup>+</sup>). The data were analysed with Flow Jo software (version10.3, Tree Star, Inc., Ashland OR, USA).

### Real-Time PCR

Total RNA was extracted from the lungs using TRIzol reagent (Invitrogen, Carlsbad, CA, USA) and then determined using Nano drop (Thermo Fisher Scientific, Waltham, MA, USA) following the manufacturer's instructions. Eligible RNA samples OD260/280 were between 1.9 and 2.0. 2 µg of complementary DNA was synthesized with the FastKing RT Kit (With gDNase) (TIANGEN, Beijing, China). Real-time PCR was performed using the QuantiNova SYBR Green PCR Kit (QIAGEN, Duesseldorf, Germany).

The following primers were used: *Stat1*, F: 5'-TCACAGTGGTTCGAGCTTCAG-3', R: 5'-GCAAACGAGACATCATAGGCA-3'; *Stat3*, F: 5'-CAATACCA TTGACCTGCCGAT-3', R: 5'-GAGCGACTCAAACCTG CCCT-3'; *Nos2*, F: 5'-CAGCTGGGCTGTACAAACCTT -3', R: 5'-CATTGGAAGTGAAGCGTTTCG-3'; *Tnf-α*, F: 5'-CTGGGAGTAGACAAGGTACAACCCAT-3', R: 5'-ATTCGAGTGACAAGCCTGTAGCCCA-3'; *Mrc1*, F: 5'-TGCAGTAACTGGTGGATTGTC-3', R: 5'-TGTTTTG GTTGGGACTGACC-3'; *β-actin*, F: 5'-TGGAATCC TGTGGCATCCATGAAAC-3', R: 5'-TAAAACGCAGCT CAGTAACAGTCCG-3'. The relative expression of target genes was measured by 2<sup>-ΔΔCt</sup> method.

### Western blot analysis

Protein samples were obtained from homogenized lung tissues. 10% SDS-polyacrylamide gel electrophoresis was used to separate various proteins. Then, the proteins were transferred to PVDF membranes. Membranes were blocked with 5% non-fat dried milk for 1 hour at room temperature and then incubated with primary antibodies against the following: p-STAT1 (Tyr701), STAT1, p-STAT3 (Tyr705), STAT3, p-MEK, MEK, p-JNK, JNK, p-ERK, ERK, p-P38, P38, p-AKT, AKT, and β-actin (all 1:1000, Cell Signalling Technology, MA, USA) overnight at 4°C. The appropriate HRP-coupled secondary antibody (1:2000, Cell Signalling Technology, MA, USA) was incubated for 1 hour at room temperature. Then the signal was detected with chemiluminescence (Millipore Corporation, MA, USA). ECL images of p-STAT1 (Tyr701), STAT1, p-STAT3 (Tyr705), and STAT3 were analysed with Image J.

### Statistical analysis

The percentage of survival rate was shown by the Kaplan – Meier method and analyses by log-rank test. Comparisons between 2 groups was analysed by student's *t*-tests. To determine statistical significance between ≥3 groups, assessment was done by ANOVA. *p* < 0.05 was considered statistically significant.

### Results

#### *pH1N1* infection-induced pathological damage and cytokine storm were infection dose- and time-dependent

To compare the changes of lung pathological damage and innate immune responses after pH1N1 infection at different doses and time, a pH1N1 infection animal model was established using TCID<sub>50</sub> of 10<sup>2</sup>/ml and 10<sup>6</sup>/ml. Following pH1N1 infection at different doses, the weight changes and survival rates were monitored for 14 days. As shown in Figure 1a,b a TCID<sub>50</sub> of 10<sup>2</sup>/ml decreased the body weight to 70% of the control group, and the survival rate was approximately 10%. A TCID<sub>50</sub> of 10<sup>6</sup>/ml induced additional body weight loss, and all mice died on the seventh dpi. Furthermore, the lungs and BALF were analysed by histology or Bio-Plex multiplex immunoassays at the indicated dpi. Histopathological analysis of the lung revealed alveolar oedema, necrosis, and haemorrhage accompanied by increased widespread inflammatory cell infiltration, alveolar epithelial cell exfoliation, and thickened alveolar walls at a TCID<sub>50</sub> of 10<sup>2</sup>/ml. More severe parenchymal destruction, alveolar cavity fusion, thickened alveolar walls, and inflammatory cell infiltration occurred following the administration of a TCID<sub>50</sub> of 10<sup>6</sup>/ml (Figure 1c-e).

Hypercytokinemia is associated with influenza virus infection and leads to greater mortality [31]. The multiplex immunoassays show that pH1N1 infection induced the elevated production of large amounts of cytokines and chemokines, including IL-6, IFNα/β/γ, TNFα, IL-1β, CXCL1, CCL2, and CCL3 in BALF, which are associated with acute lung injury (Figure 1f, Supplementary Figure S1A). The levels of IL-6, IFNα, IFNγ, TNFα, and CXCL1 in serum were also significantly increased (Figure 1g, Supplementary Figure S1B). Compared with low-dose infection, the high-dose infection induced a more robust and earlier cytokine storm, and the peak of their concentrations was advanced from 3–5 dpi to 1–3 dpi (Figure 1f,g Supplementary Figure S1A-B). Throughout the time course of infection, the virus titre and the expression

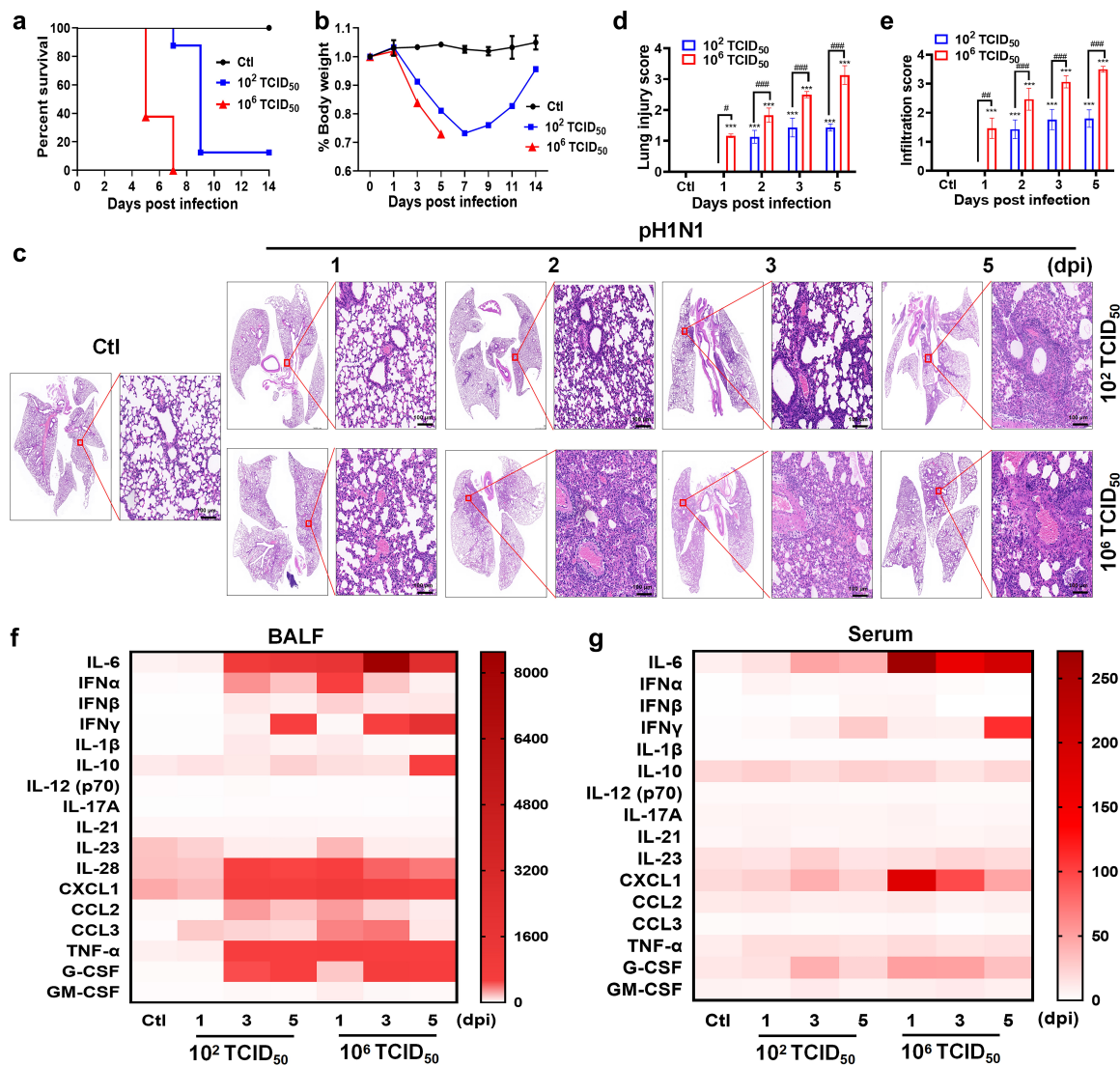


**Figure 1.** pH1N1 infection-induced pathological damage and cytokine storm were infection dose- and time-dependent. (A) Survival rate and (B) body weight change after infection with 10<sup>2</sup> TCID<sub>50</sub> and 10<sup>6</sup> TCID<sub>50</sub> pH1N1. Data are representative of two independent experiments (n = 8 for each group). (C) Lung tissue injury was assessed by H&E staining at 1, 2, 3, and 5 dpi after infecting with 10<sup>2</sup> TCID<sub>50</sub> and 10<sup>6</sup> TCID<sub>50</sub> pH1N1. Scale bar = 100  $\mu$ m; original magnification =  $\times$ 200. Semiquantitative histological scoring of lung injury (D) and infiltration (E). The heatmap of the concentration of cytokines and chemokines in the BALF (F) and serum (G) of both doses of infected mice at the indicated dpi. Data are representative of two independent experiments and presented as mean  $\pm$  SD (n = 3 for each group). In Figure D and E, # and ### represent  $p < 0.05$ ,  $p < 0.001$ , respectively, when the 10<sup>2</sup> TCID<sub>50</sub> group is compared to the 10<sup>6</sup> TCID<sub>50</sub> group. \*\*\* represents  $p < 0.001$  when the different dpi of 10<sup>2</sup> TCID<sub>50</sub> and 10<sup>6</sup> TCID<sub>50</sub> are compared to the control group. Ctl = control; dpi = days post infection.

of HA were detected. As shown in Supplementary Figure S1C, more infectious viruses could be detected in high-dose infection group at 2, 3 and 5 dpi. Immunohistochemical detection of HA was also assayed in low-dose infection group. As shown in Supplementary Figure S1D, the number of HA positive cells was gradually elevated and peaked at 5 dpi. These results suggested that high-dose pH1N1 infection induced robust and earlier cytokine storms and were associated with severe lung immunopathological damage and high mortality.

### **pH1N1 infection dose- and time-dependent recruited neutrophils into the lung**

Neutrophil activation not only functions as a defender against infections, but it also causes tissue damage and leads to inflammatory diseases [32]. With the significantly increased G-CSF, CXCL1, and CCL2, neutrophils can rapidly migrate to inflamed lung tissue. The percentage of neutrophils was analysed by flow cytometry and immunohistochemistry at the indicated dpi in response to different

infection doses. The gating strategy was shown in Supplementary Figure S2. As the infection progressed, a large number of neutrophils was immediately recruited into the lungs and peaked at 2–3 dpi (Figure 2a-b). In the high-dose infection group, significantly more neutrophils were recruited and maintained for a longer time (Figure 2a-b). The recruitment of neutrophils was further detected and confirmed by immunohistochemistry and showed similar results (Figure 2c-d). These results demonstrated that high-dose pH1N1 infection induced higher numbers and sustained recruitment of neutrophils contributed to severe lung immunopathological damage. It may help us understand the threshold at which protective functions give way to immunopathology.

### Recruitment of macrophages into the lungs was infection dose- and time-dependent and higher ratio of M1/M2 was polarized in the high-dose infection group

Macrophages are essential to maintaining lung homeostasis by initiating protective immune responses to pathogens and preventing excessive inflammatory responses via the balance between pro- and anti-inflammatory M1/M2 subsets [16,17]. However, persistent inflammation in macrophages also triggers an overexuberant inflammatory response and tissue damage by shifting to a high ratio of M1/M2 [33]. Our results also showed significantly high concentrations of CXCL1, CCL2 and CCL3 in BALF, which can recruit macrophages (Figure 1f, Supplementary Figure

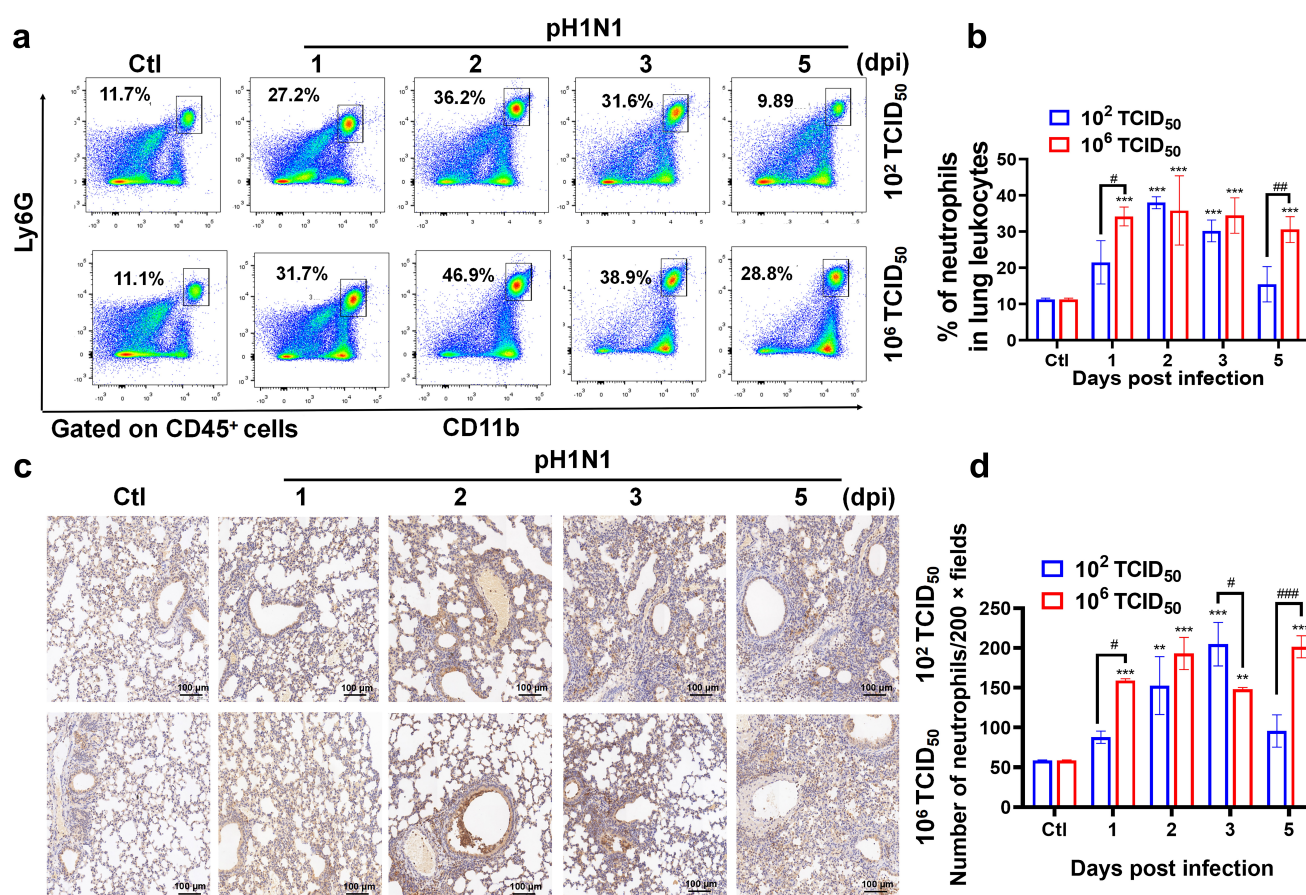


**Figure 2.** pH1N1 infection dose- and time-dependent recruited neutrophils into the lung. (A and B) the percentages of CD45<sup>+</sup>CD11b<sup>+</sup>Ly6G<sup>+</sup> neutrophils in the lungs were detected using flow cytometry at 1, 2, 3, and 5 dpi after being infected with 10<sup>2</sup> TCID<sub>50</sub> and 10<sup>6</sup> TCID<sub>50</sub> pH1N1. (C) Representative immunohistochemical images of Ly6G expression in the lungs of mice following both doses at indicated dpi. Scale bar = 100  $\mu$ m; original magnification =  $\times$ 200. (D) Quantitative analysis of Ly6G positive cells in the lung slices at the indicated dpi. Data are representative of two independent experiments and presented as mean  $\pm$  SD (n = 3 for each group). In Figure B and D, # and ### represent  $p < 0.05$  and  $p < 0.001$ , respectively, when the 10<sup>2</sup> TCID<sub>50</sub> group is compared to the 10<sup>6</sup> TCID<sub>50</sub> group. \*\* and \*\*\* represent  $p < 0.01$  and  $p < 0.001$ , respectively, when the different dpi of 10<sup>2</sup> TCID<sub>50</sub> and 10<sup>6</sup> TCID<sub>50</sub> are compared to the control group. Ctl = control; dpi = days post infection.

S1A). The percentage of macrophages was determined by flow cytometry and immunohistochemistry at the indicated dpi in response to different infection doses. The gating strategy is shown in Supplementary Figure S2. As the infection progressed, macrophages were recruited to the lungs gradually, and significantly more macrophages were recruited to the lungs in the high-dose infection group at 5 dpi than the low-dose (Figure 3a-b). A similar result was further confirmed by immunohistochemistry (Figure 3c-d).

The polarization of macrophages in response to different infection doses and time was further detected. The results show that low-dose pH1N1 infection gradually increased M1 macrophage marker genes *Nos2* and *Tnf- $\alpha$*  and peaked at 3 dpi (Figure 4a) and gradually decreased M2 macrophage marker

genes *Mrc1* (Figure 4b) [24,34]. Similarly, high-dose infection also induced gradually increased *Nos2* and *Tnf- $\alpha$* , but the peak of *Nos2* and *Tnf- $\alpha$*  was advanced to 2 dpi and 1 dpi, respectively (Figure 4a). High-dose infection induced a more significant reduction of *Mrc1* than low-dose infection at 1, 2, and 3 dpi (Figure 4b). Furthermore, flow cytometry was also used to detect the polarization of macrophages in the lung at the indicated time. As shown in Figure 4c,e the ratio of M1 macrophages was significantly elevated and peaked at 3 dpi, and the ratio of M2 was gradually reduced after low-dose infection. Similarly, high-dose infection showed a gradually elevated proportion of M1 and reduced proportion of M2 macrophages. However, the peak of M1 was advanced to 1 dpi, the ratio of M1 was significantly increased, and the ratio

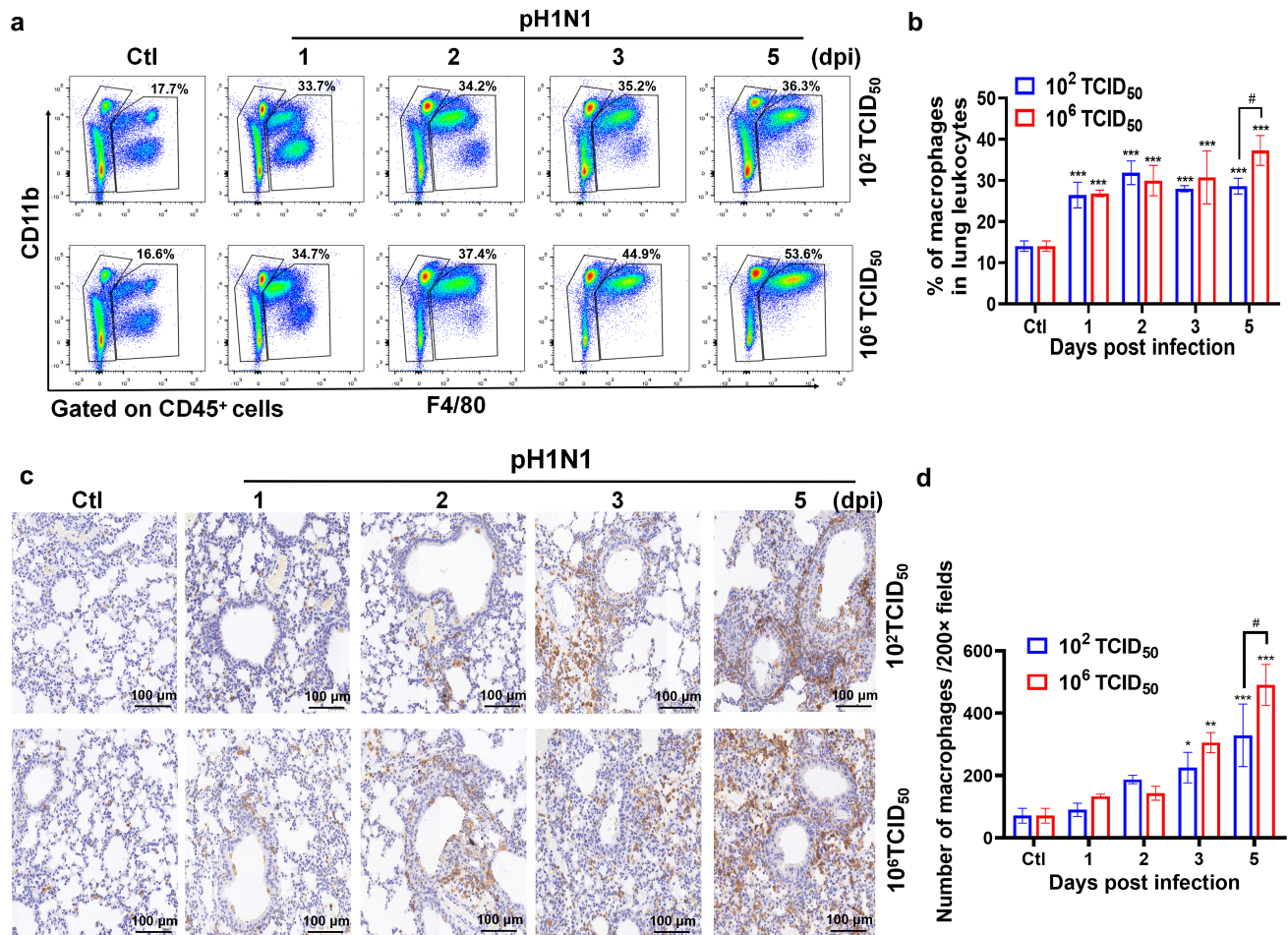


**Figure 3.** Dose- and time-dependent pH1N1 infection recruited macrophages into the lungs. (A and B) the percentages of CD45<sup>+</sup>F4/80<sup>+</sup> macrophages in the lungs were detected using flow cytometry at 1, 2, 3, and 5 dpi after being infected with 10<sup>2</sup> TCID<sub>50</sub> and 10<sup>6</sup> TCID<sub>50</sub> pH1N1. (C) Representative immunohistochemical images of F4/80 expression in the lungs of mice following both doses at the indicated dpi. Scale bar = 100  $\mu$ m, original magnification =  $\times$ 200. (D) Quantitative analysis of F4/80<sup>+</sup> cells in the lung slices at the indicated dpi. Data are representative of two independent experiments and presented as mean  $\pm$  SD (n = 3 for each group). In Figure B and D, # and ### represent  $p < 0.05$  and  $p < 0.001$ , respectively, when the 10<sup>2</sup> TCID<sub>50</sub> group is compared to the 10<sup>6</sup> TCID<sub>50</sub> group. \*\* and \*\*\* represent  $p < 0.01$  and  $p < 0.001$ , respectively, when the different dpi of 10<sup>2</sup> TCID<sub>50</sub> and 10<sup>6</sup> TCID<sub>50</sub> are compared to the control group. Ctl = control; dpi = days post infection.

of M2 was significantly decreased after high-dose infection (Figure 4c-e). The M1/M2 is more representative of the pro-inflammatory state of macrophages [35]. Our results showed that pH1N1 infection gradually increased the ratio of M1 and M2, but the ratio of M1 and M2 was more significant in the high-dose infection group than that in the lower-dose group (Figure 4f). These results demonstrated that high-dose pH1N1 infection recruited more macrophages into the lungs and induced a higher ratio of M1/M2,

which may help us understand the beneficial-to-detrimental transition and regulate immunopathological damage.

### *pH1N1* infection dose- and time-dependent activated *STAT1* and *STAT3*

As there is a significantly elevated expression of IL-6, IFNs, and G-CSF in BALF, their intracellular signalling

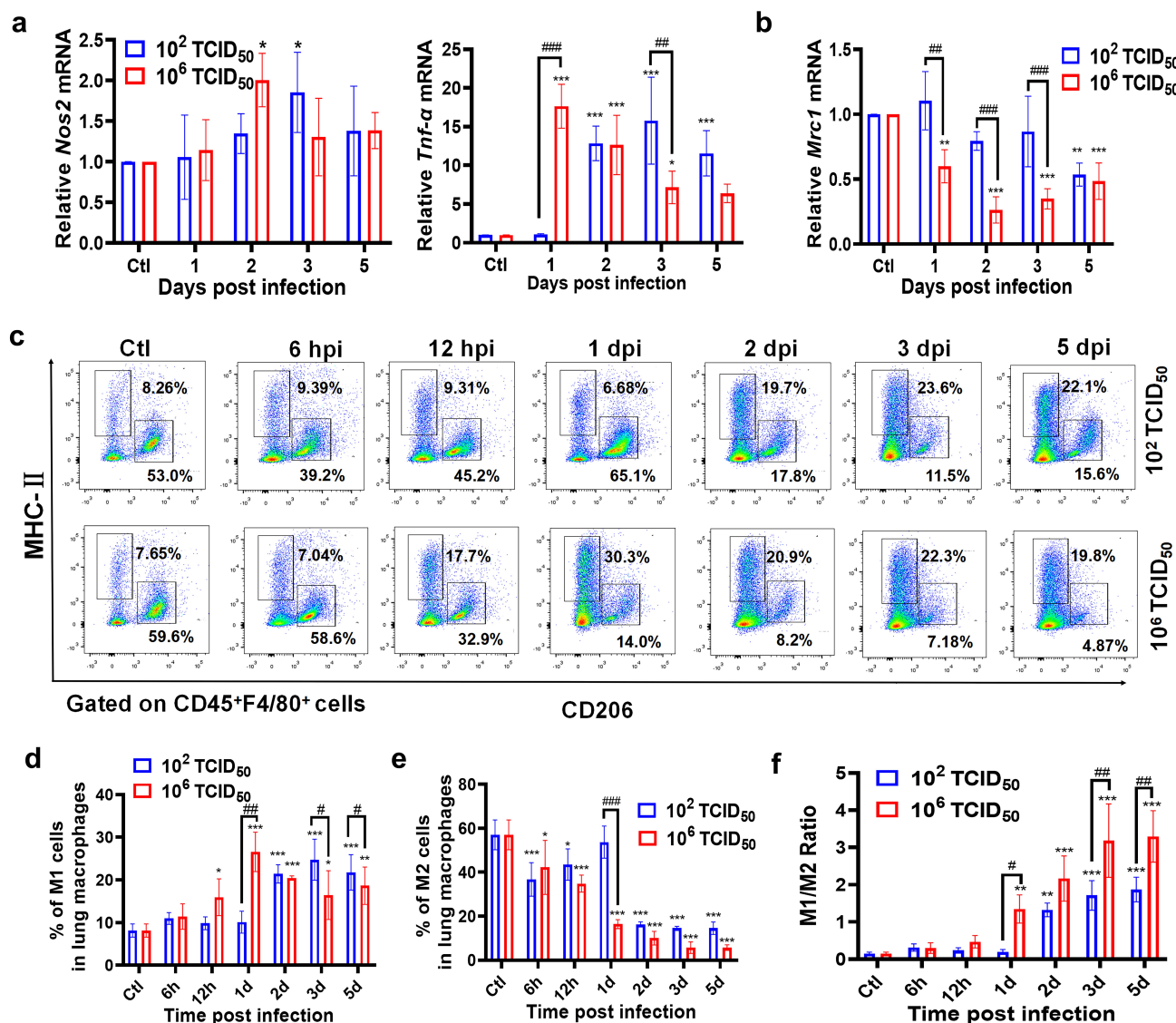


**Figure 4.** pH1N1 infection dose- and time-dependent induced higher ratio of M1/M2. (A – B) Real-time PCR analysis of *Nos2*, *Tnf-α*, and *Mrc1* in the lungs of mice at 1, 2, 3, and 5 dpi after being infected with 10<sup>2</sup> TCID<sub>50</sub> and 10<sup>6</sup> TCID<sub>50</sub> pH1N1. (C) The percentages of CD45<sup>+</sup>F4/80<sup>+</sup>MHC-II<sup>+</sup> and CD45<sup>+</sup>F4/80<sup>+</sup>CD206<sup>+</sup> macrophages in the lungs were detected using flow cytometry at 6 hpi, 12 hpi, 1 dpi, 2 dpi, 3 dpi, and 5 dpi. (D – E) The histograms show the proportion changes of M1 (F4/80<sup>+</sup>MHC-II<sup>+</sup>) and M2 (F4/80<sup>+</sup>CD206<sup>+</sup>) at different time points of infection. (F) The ratios of M1/M2 at different time points of infection. Data are representative of two independent experiments and are presented as mean ± SD (n = 3 for each group). In Figure A, B, D, E, and F, #, ##, and ### represent  $p < 0.5$ ,  $p < 0.01$ , and  $p < 0.001$ , respectively, when the 10<sup>2</sup> TCID<sub>50</sub> group is compared to the 10<sup>6</sup> TCID<sub>50</sub> group. \*, \*\*, and \*\*\* represent  $p < 0.5$ ,  $p < 0.01$ , and  $p < 0.001$ , respectively, when the different dpi of 10<sup>2</sup> TCID<sub>50</sub> and 10<sup>6</sup> TCID<sub>50</sub> are compared to the control group. Ctl = control; hpi = hours post infection; dpi = days post infection.

pathways can be activated and mediate corresponding functions. Here, the expression and activation of STAT, mitogen-activated protein kinase (MAPK), and the protein kinase B (AKT) signalling pathway, including STAT1, STAT3, MEK, JNK, ERK, p38, and AKT, in whole lung tissues were detected. pH1N1 infection significantly increased and then gradually declined transcription of STAT1 (Figure 5A). Compared with low-

dose infection, the peak of the high-dose infection group was advanced from 2 or 3 dpi to 1 dpi (Figure 5A). However, high- or low-dose pH1N1 infection only induced slightly elevated transcription of STAT3 at 1 dpi (Figure 5B). Meanwhile, pH1N1 progressively increased STAT1 expression regardless of infectious dose, and high-dose infection induced an earlier significant increase in STAT1 expression.

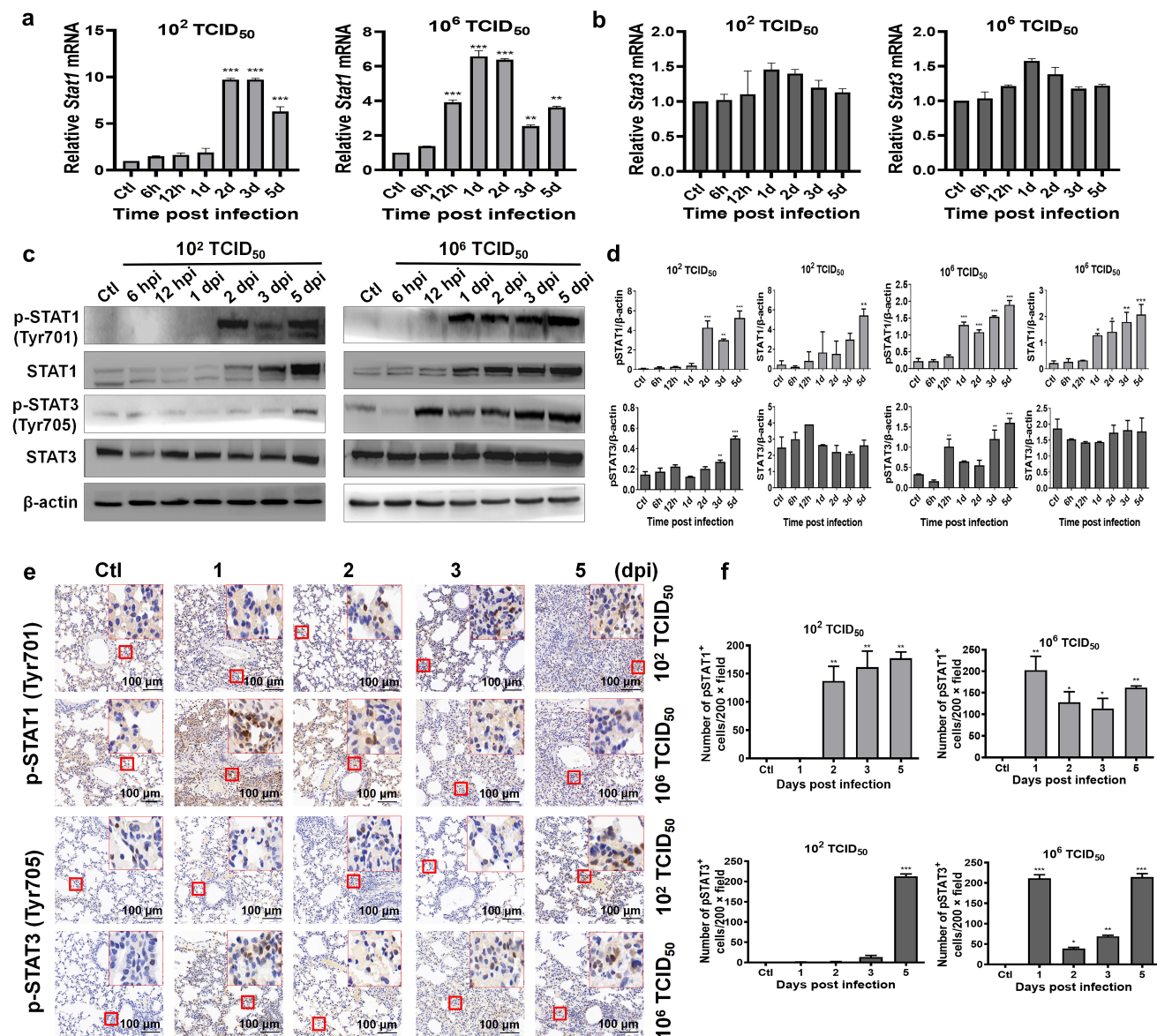


**Figure 5.** pH1N1 infection dose- and time-dependent activated STAT1 and STAT3. Real-time PCR analysis of the *Stat1* (A) and *Stat3* (B) in the lungs of mice at 6 hpi, 12 hpi, 1 dpi, 2 dpi, 3 dpi, and 5 dpi after being infected with  $10^2$  TCID<sub>50</sub> and  $10^6$  TCID<sub>50</sub> pH1N1. (C) Western blot analysis of p-STAT1 (Tyr701), STAT1, p-STAT3 (Tyr705), and STAT3 expression in the lungs of different treatment groups at the indicated time post infection. (D) The expression of p-STAT1 (Tyr701), STAT1, p-STAT3 (Tyr705), and STAT3 relative to β-actin at the indicated time post-infection of different treatment groups. (E) Representative immunohistochemical images of p-STAT1 (Tyr701) and p-STAT3 (Tyr705) expression in the lungs of mice following both doses at the indicated dpi. Scale bar = 100 μm; original magnification = ×200. (F) Quantitative analysis of p-STAT1 (Tyr701) and p-STAT3 (Tyr705) positive cells in the lung slices at the indicated dpi. Data are representative of two independent experiments and are presented as mean ± SD (n = 3 for each group). In Figure A, B, D, and F, \*, \*\*, and \*\*\* represent  $p < 0.05$ ,  $p < 0.01$ , and  $p < 0.001$ , respectively, when the different dpi of  $10^2$  TCID<sub>50</sub> and  $10^6$  TCID<sub>50</sub> are compared to the control group. Ctl = Control; hpi = hours post infection; dpi = days post infection.

Similarly, the expression of STAT3 was constant regardless of infection doses (Figure 5C,D). To detect their activation, the phosphorylation of STAT1/3 was also assayed.

As shown in Figure 5C,D the expression of p-STAT1 (Tyr701) was significantly increased from 2 dpi by low-dose infection, but their significant increase advanced to 1 dpi. Similarly, the expression of p-STAT3 (Tyr705) was significantly increased at 5 dpi by low-dose infection, but their hyperactivation advanced to 0.5 dpi. The phosphorylation and nuclear localization of STAT1/3 were further confirmed by immunohistochemistry and showed similar results (Figure 5E-F). Although the expression of MEK, JNK, p38, ERK, and AKT, did not show obvious change, the activation of p-JNK was significantly increased after infection, and high-dose pH1N1 induced the earlier activation. AKT activation was only progressively increased by high-dose infection. The activation of p-MEK and p-P38 show acute elevation at 0.5 dpi and 2–3 dpi. The activation of p-ERK was gradually impaired after infection (Supplementary Figure S3). These results suggested that STAT1 and STAT3 were activated after pH1N1 infection, and high-dose pH1N1 infection induced robust and earlier activation, which may be associated with the beneficial immunoprotective or detrimental immunopathological.

### ***Inhibition of STAT1 and/or STAT3 aggravated low-dose pH1N1 infection induced lung damage and decreased survival rate***

The expression of IFNs and activation of STAT1/3 may play antiviral immune protection or immunopathological damage. Our previous reports found that neutralization of IFN $\gamma$  in high-dose infection can alleviate pathological damage [27]. Whether STAT1 and STAT3 have a protective or deleterious role during low-dose infection still needs further study. To better simulate the clinical case and situation, delayed oseltamivir and/or STAT1/3 inhibitor treatment at 2 dpi in a low-dose infection mice model was shown as a schematic diagram in Figure 6A.

As shown in Figure 6B, Fludarabine, C188–9, or Stattic monotherapy had no effect on the survival rate of uninfected mice. The survival rate of mice in the DMSO-treated control group was 40% after  $10^2$  TCID $_{50}$  of pH1N1 infection. Delayed Oseltamivir monotherapy can improve the survival rate to 75%. However, delayed Fludarabine, C188–9, or Stattic monotherapy significantly reduced their survival rates to 10.5%, 12.5%, and 0%, respectively (Figure 6B).

Combined therapy with delayed Oseltamivir and Fludarabine or C188–9 did not confer any additional survival rate benefit compared to Oseltamivir monotherapy. Conversely, combined therapy with delayed Oseltamivir and Stattic exacerbated the survival rate more than delayed Oseltamivir monotherapy (Figure 6B). Consistent with the survival rate data, bodyweight loss in delayed Fludarabine, C188–9, or Stattic treatment groups were more than Oseltamivir treatment (Figure 6C). Pathological damage in the lungs was also assessed and shown in Figure 6D, DMSO-treated pH1N1-infected lungs showed excessive lung damage, including diffused alveolar damage, inflammatory infiltration and desquamation of bronchiolar epithelial cells.

Delayed Oseltamivir monotherapy merely alleviated pathological damage slightly, whereas delayed Fludarabine, C188–9, or Stattic monotherapy obviously aggravated lung pathological injury, and combined therapy also could not ameliorate lung pathological injury compared to the control (Figure 6D). These results demonstrate that the inhibition of STAT1/3 with delayed Fludarabine, C188–9, or Stattic treatment did not provide survival benefits and pathological improvement against  $10^2$ /ml TCID $_{50}$  pH1N1 infection.

## **Discussion**

The emergence of pH1N1 in 2009 caused a pandemic all over the world. Annual and occasional pandemics of H1N1 viruses pose a significant health risk to people worldwide. Mild influenza virus infection sees recovery with a modest immune response. Our clinical data and mouse model experiments revealed that severe pH1N1 infection presents with rapidly progressive pneumonia characterized by extensive and diffuse alveolar damage and multiple organ failures [3,9–11,13,36]. Respiratory distress associated with immunopathological lesions is the main cause of death in severely infected patients [14,36]. We and others have found that exacerbated pulmonary inflammatory response-induced immunopathological damage plays a critical actor in the pathogenesis of severe pneumonia, providing novel strategies and targets for the treatment of severe influenza infection [3,10,11,14,15,36]. Rational host innate immune system constitutes the first line of defence to eliminate influenza virus and maintain immune homeostasis.

An aberrant innate immune response is thought to play an important actor in severe respiratory infection [37]. Comparing of pH1N1-induced innate immune responses, including neutrophils, macrophages, virus titres, cytokines/chemokines, and key signalling pathway molecules at the indicated dpi of different

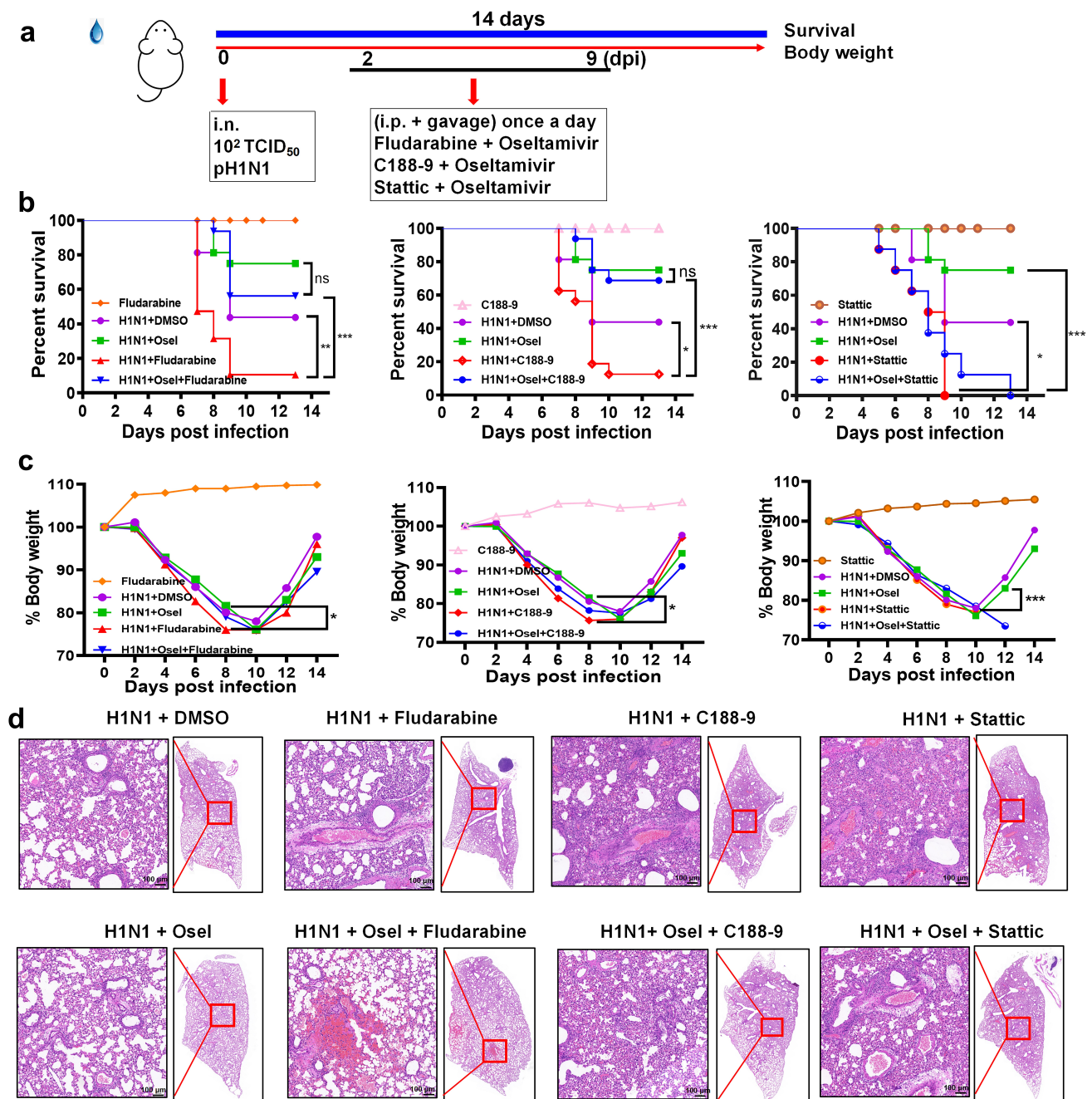


**Figure 6.** Inhibition of STAT1 and/or STAT3 aggravated low-dose pH1N1 infection-induced lung damage and decreased survival rate. (A) BALB/c mice were infected with  $10^2$  TCID<sub>50</sub> doses of pH1N1 and treated by different drug combinations at 2 dpi for 7 days. Survival rate (B) and body weight changes (C) following treatment with Fludarabine/C188-9/stattic, DMSO, Osetamivir, Osetamivir + Fludarabine, Osetamivir + C188-9/stattic or Osetamivir + Fludarabine, Osetamivir + C188-9 or Osetamivir + Stattic. (D) Lung tissue injury was assessed by H&E staining. Data are representative of two independent experiments ( $n = 8-16$  for each group). In Figure B and C, \*, \*\*, and \*\*\* represent  $p < 0.05$ ,  $p < 0.01$ , and  $p < 0.001$ , respectively, when comparing the different treatment groups. Osel = Osetamivir.

infectious doses is helpful to understand their immunoprotective or immunopathological effects. It also helps us understand the threshold at which protective functions give way to immunopathology and provides us with potential adjunctive therapeutic targets and strategies for alleviating influenza-induced pneumonia.

In this study, the differences of neutrophils, macrophages, cytokines/chemokines, virus titres, and key signalling pathway molecules mediated innate immune responses and were detected using a mice model of  $10^2/\text{ml}$  and  $10^6/\text{ml}$  TCID<sub>50</sub> at the indicated days post infection. Our results demonstrated that the degree of

pathological damage is related to the pH1N1 infectious dose and time, massive numbers and more sustained neutrophil infiltration, the preferred M1 macrophage polarization, more infectious viruses, robust and earlier cytokine storm, and their activated STAT1 and STAT3 are associated with high-dose infection, which induced more severe lung immunopathological damage. The inhibition of STAT1 and/or STAT3 with Fludarabine, C188-9, or Stattic aggravated low-dose pH1N1 infection induced lung damage and decreased survival rate. The beneficial or detrimental effects of innate immune responses are in an infection time- and dose-dependent manner. The severe innate immune responses are the key reason that protective functions give way to immunopathology. The double-edged sword function of the innate immune responses should be considered when choosing the adjunctive immunomodulatory therapy for alleviating influenza-induced pneumonia.

Neutrophils are the pivotal innate immune cell of defence against bacterial, fungal, and viral infections. Neutrophils circulate in blood vessels and can rapidly infiltrate the inflamed lungs of the infection, and they exhibit a extensive range of effector functions to eliminate pathogens, including phagocytosis, production of reactive oxygen species (ROS), degranulation, and the formation of neutrophil extracellular traps [38]. However, while moderate neutrophil response can promote infection resolution [39], excessive neutrophil activation also contributes to the tissue damage of severe disease during the inflammatory process [40–42]. Because neutrophil recruitment to the lungs is related to disease severity during viral infections, neutrophils have been considered as the key role of disease pathogenesis [40,43]. Thus, the functions of neutrophils in influenza viral infection is complex, and the threshold at which protective effects give way to immunopathology is not well understood. Our experimental results show that high-dose infection induced both higher levels and earlier expression of CXCL1, which may with chemotaxis recruit more neutrophils over a longer period. Excessive and sustained neutrophil recruitment in the lungs is associated with more serious disease. To reduce neutrophil inflammation, further research is needed to investigate the mechanisms by which neutrophils exacerbate disease severity.

The pulmonary macrophage is another prominent innate immune cell to combat infection and maintain immune homeostasis. After pH1N1 infection, monocyte-derived macrophages which circulated in blood can be recruited to the lungs. Mature macrophages can switch their phenotypes and undergo functional polarization. M1 macrophages produce elevated levels of ROS and pro-inflammatory cytokines, such as IL-1 $\beta$ ,

IL-6, IL-12, IL-23, and TNF- $\alpha$ , promote pathogen clearance and regulate local immune responses. M2 macrophages produce anti-inflammatory cytokines, such as IL-10 and TGF- $\beta$ , to repair tissue and resolute inflammatory responses [44,45]. The equilibrium between the elimination of pathogens and the magnitude of the host response is critical for maintaining immune homeostasis. A well-coordinated macrophage response can effectively eliminate pathogens [44,45]. However, dysregulated macrophage activation is also a key driver of the progression of viral infections and disease.

Our results showed that the virus was replicating in lung tissue, which were consistent with the lung pathology. The results suggested that the pathogen associated molecular pattern (PAMP) of virus can induce pattern recognition receptor (PRR) activation and cytokine release during the time course of infection. The virus maybe inactivated by cytokines (IFNs), phagocytic cells, antibodies and cytotoxic cells, as well as inducing immune pathological damage.

Our results showed that large amounts of macrophages immediately recruit into the lungs after pH1N1 infection, which is consistent with the high concentration of chemokines CCL2, CCL3, and CXCL1 in BALF. Changes in different macrophage subsets, such as alveolar macrophages, inflammatory monocytes, and interstitial macrophages, should be further investigated. High-dose infections did not make a noticeable difference on macrophage compared to neutrophils. Functionally polarized subpopulations are more relevant to the physiological and pathological functions of macrophages.

Our results suggested that an excessive or a prolonged ratio of M1/M2 can lead to tissue injury and contribute to pathogenesis. Dysregulated macrophages also initiate uncontrolled cytokine release and develop cytokine storms. Blocking the development of cytokine storms may be an effective approach to improve patient outcomes, but therapies that target individual cytokines show a limited function due to the multiple of cytokines involved in the process of infection. Dysfunctional balance of M1/M2 macrophage polarization appears to play an important actor in the development of cytokine storm. As potential treatment strategies, therapeutic interventions targeting these cells may be a more effective method than targeting specific cytokines, and they may demonstrate beneficial in alleviating the cytokine storm-induced pathology and mortality of severe infections.

In addition to dysfunctional macrophages (the main source cells of inflammatory cytokines), their common signalling pathway is another potential therapeutic target and strategy. The STAT1 and STAT3 are critical transcription factors of the hallmark pro-inflammatory cytokines of IL-6, IFNs, TNF- $\alpha$ , and G-CSF in BALF

after influenza virus infection. STAT1, as a molecule that responds to either IFN $\alpha$  or IFN $\gamma$ , can resolve infections by viruses. The IFN response protects from viral infection by inducing lots of interferon-stimulated genes (ISGs), some of which encode antiviral effectors [46]. Influenza-induced pulmonary inflammation is enhanced in *Stat1*<sup>-/-</sup> mice [47]. Mice with disruption of STAT1 Y701 phosphorylation suppresses anti-influenza response [48]. Patients with STAT1 mutation are more susceptible to infection with mycobacteria and specific pathogenic virus [49]. Fludarabine can be used as a single drug or in combination with other agents for the treatment of HIV-1 and hematological disorders [50,51].

However, it was also reported that the inhibition of STAT1 with Fludarabine improved the survival rate, decreased body weight loss, and alleviated lung damage in severe influenza virus infection [52]. We and other groups have found that STAT3 is highly activated after influenza virus infection [53,54]. The inhibition of STAT3 phosphorylation in H1N1 PR8 influenza virus-infected BMDM can reduce the viral load [55]. To further confirm the therapeutic effects of the STAT3 and STAT1 inhibitor, we also evaluated the immunomodulatory effects of Fludarabine, C188-9, and Stattic during low-dose pH1N1 infection. In clinical situation, patients usually cannot receive treatment until 2 dpi or even later after the occurrence of symptoms after infection. Delayed therapy used in the mouse model can better simulate the clinical settings [4].

However, the treatment with STAT1 and/or STAT3 inhibitors after low-dose pH1N1 infection will aggravate pH1N1 virus-induced pathological damage, which is manifested by the worsening of survival rate and weight loss as well as the aggravation of immunopathology in mice. This illustrates the potential protective effect of STAT1/3 in the 10<sup>2</sup>/ml TCID<sub>50</sub> dose of pH1N1 infection. These data indicated that the immunoprotective or immunopathological effects of STAT1 *in vivo* depend on the virus strain, infectious dose, and treatment time. Comprehensive assessment of the magnitude of the host immune response after infection is essential for the application of STAT1/3 inhibitors for the treatment of pH1N1 infection. The signalling pathway of Raf/MEK/ERK is a prerequisite for influenza virus replication. Furthermore, the inhibition of this intracellular signalling pathway leads to reduction of influenza virus load [56]. We also found MEK, JNK and P38 were activated, which may be associated with pH1N1 replication.

In conclusion, our results demonstrated that pH1N1 infection induced robust and earlier pathological damage, and cytokine storm is infection

dose- and time-dependent. High-dose pH1N1 infection induced stronger and earlier innate immune responses, including the massive and sustained recruitment of neutrophils, dysregulated polarization of M1/M2, excessive and earlier cytokine storm and STAT1 and STAT3 activation. They also contributed to severe lung immunopathological damage. STAT1 and/or STAT3 function has an immunoprotective role during low-dose pH1N1 infection. Our results that suggested the beneficial or detrimental effects of innate immune response is infection time- and dose-dependent. Comprehensive assessment of the magnitude of the host innate immune responses at which protective functions give way to immunopathology is essential for adjunctive immunomodulatory therapy to alleviate influenza-induced pneumonia.

## Disclosure statement

No potential conflict of interest was reported by the author(s).

## Funding

This subject was supported by grants from National Natural Science Foundation of China [82071747, 81373114], Beijing Natural Science Foundation [7182013], Project of High-level Teachers in Beijing Municipal Universities in the Period of 13th Five-year Plan [IDHT20190510], and Taishan Scholars Program of Shandong Province [tsqn202103196].

## Data availability

The authors confirm that the data supporting the findings of this subject are available within the article and its supplementary materials.

## Ethics statement

All experiments were conducted in compliance in biosafety level 3 facilities with the approval of governmental and institutional guidelines. The experiments were performed with the Institutional Animal Care and Use Committee (IACUC) of Capital Medical University.

## References

- [1] Taubenberger JK, Morens DM. Influenza: the once and future pandemic. *Public Health Rep.* 2010;125(3):16–26.
- [2] Taubenberger JK, Kash JC. Influenza virus evolution, host adaptation, and pandemic formation. *Cell Host Microbe.* 2010;7(6):440–451. DOI:10.1016/j.chom.2010.05.009
- [3] Wu X, Bao L, Hu Z, et al. Ficolin A exacerbates severe H1N1 influenza virus infection-induced acute lung

- immunopathological injury via excessive complement activation. *Cell Mol Immunol.* **2021**;18(9):2278–2280. DOI:10.1038/s41423-021-00737-1
- [4] Jia X, Liu B, Bao L, et al. Delayed oseltamivir plus sirolimus treatment attenuates H1N1 virus-induced severe lung injury correlated with repressed NLRP3 inflammasome activation and inflammatory cell infiltration. *PLoS Pathog.* **2018**;14(11):e1007428. DOI:10.1371/journal.ppat.1007428
- [5] de Jong MD, Simmons CP, Thanh TT, et al. Fatal outcome of human influenza A (H5N1) is associated with high viral load and hypercytokinemia. *Nat Med.* **2006**;12(10):1203–1207. DOI:10.1038/nm1477
- [6] Xue C, Wen M, Bao L, et al. Vgamma4(+) gammaDelta cells aggravate severe h1n1 influenza virus infection-induced acute pulmonary immunopathological injury via secreting interleukin-17A. *Front Immunol.* **2017**;8:1054. DOI:10.3389/fimmu.2017.01054
- [7] Koutsakos M, Kedzierska K, Subbarao K. Immune responses to avian influenza viruses. *J Immunol.* **2019**;202(2):382–391. DOI:10.4049/jimmunol.1801070
- [8] Fajgenbaum DC, June CH. Cytokine storm. *N Engl J Med.* **2020**;383(23):2255–2273. DOI:10.1056/NEJMr2026131
- [9] Ichiyama T, Isumi H, Ozawa H, et al. Cerebrospinal fluid and serum levels of cytokines and soluble tumor necrosis factor receptor in influenza virus-associated encephalopathy. *Scand J Infect Dis.* **2003**;35(1):59–61. DOI:10.1080/0036554021000026986
- [10] Channappanavar R, Fehr AR, Zheng J, et al. IFN-I response timing relative to virus replication determines MERS coronavirus infection outcomes. *J Clin Invest.* **2019**;129(9):3625–3639. DOI:10.1172/JCI126363
- [11] Cilloniz C, Pantin-Jackwood MJ, Ni C, et al. Lethal dissemination of H5N1 influenza virus is associated with dysregulation of inflammation and lipoxin signaling in a mouse model of infection. *J Virol.* **2010**;84(15):7613–7624. DOI:10.1128/JVI.00553-10
- [12] Karki R, Sharma BR, Tuladhar S, et al. Synergism of TNF-alpha and IFN-gamma triggers inflammatory cell death, tissue damage, and mortality in SARS-CoV-2 infection and cytokine shock syndromes. *Cell.* **2021**;184(1):149–168. DOI:10.1016/j.cell.2020.11.025
- [13] La Gruta NL, Kedzierska K, Stambas J, et al. A question of self-preservation: immunopathology in influenza virus infection. *Immunol Cell Biol.* **2007**;85(2):85–92. DOI:10.1038/sj.icb.7100026
- [14] Zhang N, Bao YJ, Tong AH, et al. Whole transcriptome analysis reveals differential gene expression profile reflecting macrophage polarization in response to influenza A H5N1 virus infection. *BMC Med Genomics.* **2018**;11(1):20. DOI:10.1186/s12920-018-0335-0
- [15] Geng P, Zhu H, Zhou W, et al. Baicalin inhibits influenza A virus infection via promotion of m1 macrophage polarization. *Front Pharmacol.* **2020**;11:1298. DOI:10.3389/fphar.2020.01298
- [16] Davis MJ, Tsang TM, Qiu Y, et al. Macrophage M1/M2 polarization dynamically adapts to changes in cytokine microenvironments in *Cryptococcus neoformans* infection. *Mbio.* **2013**;4(3):e213–64. DOI:10.1128/mBio.00264-13
- [17] Lawrence T, Natoli G. Transcriptional regulation of macrophage polarization: enabling diversity with identity. *Nat Rev Immunol.* **2011**;11(11):750–761. DOI:10.1038/nri3088
- [18] Mosser DM, Edwards JP. Exploring the full spectrum of macrophage activation. *Nat Rev Immunol.* **2008**;8(12):958–969. DOI:10.1038/nri2448
- [19] Ren Y, Khan FA, Pandupuspitasari NS, et al. Immune evasion strategies of pathogens in macrophages: the potential for limiting pathogen transmission. *Curr Issues Mol Biol.* **2017**;21:21–40.
- [20] Schneider WM, Chevillotte MD, Rice CM. Interferon-Stimulated genes: a complex web of host defenses. *Annu Rev Immunol.* **2014**;32(1):513–545. DOI:10.1146/annurev-immunol-032713-120231
- [21] Yan Z, Gibson SA, Buckley JA, et al. Role of the JAK/STAT signaling pathway in regulation of innate immunity in neuroinflammatory diseases. *Clin Immunol.* **2018**;189:4–13. DOI:10.1016/j.clim.2016.09.014
- [22] Ivashkiv LB, Hu X. Signaling by STATs. *Arthritis Res Ther.* **2004**;6(4):159–168. DOI:10.1186/ar1197
- [23] Ji L, Zhao X, Zhang B, et al. Slc6a8-Mediated creatine uptake and accumulation reprogram macrophage polarization via regulating cytokine responses. *Immunity.* **2019**;51(2):272–284. DOI:10.1016/j.immuni.2019.06.007
- [24] Huangfu N, Zheng W, Xu Z, et al. RBM4 regulates M1 macrophages polarization through targeting STAT1-mediated glycolysis. *Int Immunopharmacol.* **2020**;83:106432. DOI:10.1016/j.intimp.2020.106432
- [25] Yin Z, Ma T, Lin Y, et al. IL-6/STAT3 pathway intermediates M1/M2 macrophage polarization during the development of hepatocellular carcinoma. *J Cell Biochem.* **2018**;119(11):9419–9432. DOI:10.1002/jcb.27259
- [26] Lee B, Gopal R, Manni ML, et al. STAT1 is required for suppression of type 17 immunity during influenza and bacterial superinfection. *Immunohorizons.* **2017**;1(6):81–91. DOI:10.4049/immunohorizons.1700030
- [27] Liu B, Bao L, Wang L, et al. Anti-IFN-Gamma therapy alleviates acute lung injury induced by severe influenza A (H1N1) pdm09 infection in mice. *J Microbiol Immunol Infect.* **2021**;54(3):396–403. DOI:10.1016/j.jmii.2019.07.009
- [28] Liu B, Zhang X, Deng W, et al. Severe influenza A (H1N1) pdm09 infection induces thymic atrophy through activating innate CD8(+)/CD44(hi) T cells by upregulating IFN-γ. *Cell Death Dis.* **2014**;5(10):e1440. DOI:10.1038/cddis.2014.323
- [29] Smith KM, Mrozek JD, Simonton SC, et al. Prolonged partial liquid ventilation using conventional and high-frequency ventilatory techniques: gas exchange and lung pathology in an animal model of respiratory distress syndrome. *Crit Care Med.* **1997**;25(11):1888–1897. DOI:10.1097/00003246-199711000-00030
- [30] Zhang J, Ma M, Qin D, et al. Lung morphometry changes in prevention of airway remodeling by protocatechuic aldehyde in asthmatic mice. *Int J Clin Exp Med.* **2015**;8(5):6890–6901.
- [31] Wei F, Gao C, Wang Y. The role of influenza A virus-induced hypercytokinemia. *Crit Rev Microbiol.*

- 2022;48(2):240–256. DOI:10.1080/1040841X.2021.1960482
- [32] Nemeth T, Sperandio M, Mocsai A. Neutrophils as emerging therapeutic targets. *Nat Rev Drug Discov.* 2020;19(4):253–275. DOI:10.1038/s41573-019-0054-z
- [33] Merad M, Martin JC. Pathological inflammation in patients with COVID-19: a key role for monocytes and macrophages. *Nat Rev Immunol.* 2020;20(6):355–362. DOI:10.1038/s41577-020-0331-4
- [34] von Ehr a, Attaai A, Neidert N, et al. Inhibition of microglial TGFβ signaling increases expression of Mrc1. *Front Cell Neurosci.* 2020;14:66. DOI:10.3389/fncel.2020.00066
- [35] Tarique AA, Logan J, Thomas E, et al. Phenotypic, functional, and plasticity features of classical and alternatively activated human macrophages. *Am J Respir Cell Mol Biol.* 2015;53(5):676–688. DOI:10.1165/rcmb.2015-0012OC
- [36] Kim KS, Jung H, Shin IK, et al. Induction of interleukin-1 beta (IL-1beta) is a critical component of lung inflammation during influenza A (H1N1) virus infection. *J Med Virol.* 2015;87(7):1104–1112. DOI:10.1002/jmv.24138
- [37] Volz E, Hill V, Mccrone JT, et al. Evaluating the effects of SARS-CoV-2 spike mutation D614G on transmissibility and pathogenicity. *Cell.* 2021;184(1):64–75. DOI:10.1016/j.cell.2020.11.020
- [38] Johansson C, Kirsebom F. Neutrophils in respiratory viral infections. *Mucosal Immunol.* 2021;14(4):815–827. DOI:10.1038/s41385-021-00397-4
- [39] Tate MD, Deng YM, Jones JE, et al. Neutrophils ameliorate lung injury and the development of severe disease during influenza infection. *J Immunol.* 2009;183(11):7441–7450. DOI:10.4049/jimmunol.0902497
- [40] Zhou Z, Ren L, Zhang L, et al. Heightened innate immune responses in the respiratory tract of COVID-19 patients. *Cell Host Microbe.* 2020;27(6):883–890. DOI:10.1016/j.chom.2020.04.017
- [41] Perrone LA, Plowden JK, Garcia-Sastre A, et al. H5N1 and 1918 pandemic influenza virus infection results in early and excessive infiltration of macrophages and neutrophils in the lungs of mice. *PLoS Pathog.* 2008;4(8):e1000115. DOI:10.1371/journal.ppat.1000115
- [42] Kulkarni U, Zemans RL, Smith CA, et al. Excessive neutrophil levels in the lung underlie the age-associated increase in influenza mortality. *Mucosal Immunol.* 2019;12(2):545–554. DOI:10.1038/s41385-018-0115-3
- [43] Tang BM, Shojaei M, Teoh S, et al. Neutrophils-Related host factors associated with severe disease and fatality in patients with influenza infection. *Nat Commun.* 2019;10(1):3422. DOI:10.1038/s41467-019-11249-y
- [44] Byrne AJ, Mathie SA, Gregory LG, et al. Pulmonary macrophages: key players in the innate defence of the airways. *Thorax.* 2015;70(12):1189–1196. DOI:10.1136/thoraxjnl-2015-207020
- [45] Shapouri-Moghaddam A, Mohammadian S, Vazini H, et al. Macrophage plasticity, polarization, and function in health and disease. *J Cell Physiol.* 2018;233(9):6425–6440. DOI:10.1002/jcp.26429
- [46] Schoggins JW, Rice CM. Interferon-Stimulated genes and their antiviral effector functions. *Curr Opin Virol.* 2011;1(6):519–525. DOI:10.1016/j.coviro.2011.10.008
- [47] Lee B, Gopal R, et al. STAT1 is required for suppression of type 17 immunity during influenza and bacterial superinfection. *Immunohorizons.* 2017;1(6):81–91. DOI:10.4049/immunohorizons.1700030
- [48] Liu S, Liao Y, Chen B, et al. Critical role of Syk-dependent STAT1 activation in innate antiviral immunity. *Cell Rep.* 2021;34(3):108627. DOI:10.1016/j.celrep.2020.108627
- [49] Vairo D, Tassone L, Tabellini G, et al. Severe impairment of IFN-gamma and IFN-alpha responses in cells of a patient with a novel STAT1 splicing mutation. *Blood.* 2011;118(7):1806–1817. DOI:10.1182/blood-2011-01-330571
- [50] Herishanu Y, Tadmor T, Braester A, et al. Low-Dose fludarabine and cyclophosphamide combined with standard dose rituximab (LD-FCR) is an effective and safe regimen for elderly untreated patients with chronic lymphocytic leukemia: the Israeli CLL study group experience. *Hematol Oncol.* 2019;37(2):185–192. DOI:10.1002/hon.2580
- [51] Chaudhuri A, Yang B, Gendelman HE, et al. STAT1 signaling modulates HIV-1-induced inflammatory responses and leukocyte transmigration across the blood-brain barrier. *Blood.* 2008;111(4):2062–2072. DOI:10.1182/blood-2007-05-091207
- [52] Zhang S, Huo C, Xiao J, et al. P-STAT1 regulates the influenza A virus replication and inflammatory response in vitro and vivo. *Virology.* 2019;537:110–120. DOI:10.1016/j.virol.2019.08.023
- [53] Zhu L, Yang P, Zhao Y, et al. Single-Cell sequencing of peripheral mononuclear cells reveals distinct immune response landscapes of COVID-19 and influenza patients. *Immunity.* 2020;53(3):685–696. DOI:10.1016/j.immuni.2020.07.009
- [54] Kwok HH, Poon PY, Fok SP, et al. Anti-Inflammatory effects of indirubin derivatives on influenza A virus-infected human pulmonary microvascular endothelial cells. *Sci Rep.* 2016;6(1):18941. DOI:10.1038/srep18941
- [55] Ampomah PB, Moraes LA, Lukman HM, et al. Formyl peptide receptor 2 is regulated by RNA mimics and viruses through an IFN-beta-STAT3-dependent pathway. *FASEB J.* 2018;32(3):1468–1478. DOI:10.1096/fj.201700584RR
- [56] Pleschka S, Wolff T, Ehrhardt C, et al. Influenza virus propagation is impaired by inhibition of the Raf/MEK/ERK signalling cascade. *Nat Cell Biol.* 2001;3(3):301–305. DOI:10.1038/35060098